

# **The *HST* Key Project on the Extragalactic Distance Scale XI. The Cepheids in NGC 4414<sup>1</sup>**

Anne Turner<sup>2</sup>, Laura Ferrarese<sup>3,4</sup>, Abhijit Saha<sup>5,6</sup>, Fabio Bresolin<sup>2,7</sup>, Robert C. Kennicutt Jr.<sup>2</sup>, Peter B. Stetson<sup>8</sup>, Jeremy R. Mould<sup>9</sup>, Wendy L. Freedman<sup>10</sup>, Brad K. Gibson<sup>9</sup>, John A. Graham<sup>11</sup>, Holland Ford<sup>12</sup>, Minsheng Han<sup>13</sup>, Paul Harding<sup>2</sup>, J. G. Hoessel<sup>13</sup>, John P. Huchra<sup>14</sup>, Shaun M. G. Hughes<sup>15</sup>, Garth D. Illingworth<sup>16</sup>, Daniel D. Kelson<sup>11</sup>, Lucas Macri<sup>14</sup>, Barry F. Madore<sup>17</sup>, Randy Phelps<sup>10</sup>, Daya Rawson<sup>9</sup>, Shoko Sakai<sup>6,17</sup>, N. A. Silbermann<sup>17</sup>

Received \_\_\_\_\_; accepted \_\_\_\_\_

---

<sup>1</sup>Based on observations with the NASA/ESA *Hubble Space Telescope*, obtained at the Space Telescope Science Institute, operated by AURA, Inc. under NASA contract No. NAS5-26555.

<sup>2</sup>Steward Observatory, University of Arizona, Tucson, AZ 85721

<sup>3</sup>California Institute of Technology, Pasadena, CA 91125

<sup>4</sup>Hubble Fellow

<sup>5</sup>Space Telescope Science Institute, Baltimore, MD 21218

<sup>6</sup>now at National Optical Astronomy Observatories, P.O. Box 26732, Tucson, AZ 85726

<sup>7</sup>now at European Southern Observatory, D-85478, Garching b. München, Germany

<sup>8</sup>Dominion Astrophysical Observatory, Victoria, British Columbia V8X 4M6, Canada

<sup>9</sup>Mount Stromlo and Siding Springs Observatories, Instituted of Advanced Studies, ANU, ACT 2611 Australia

<sup>10</sup>Observatories of the Carnegie Institution of Washington, Pasadena, CA 91101

<sup>11</sup>Dept. of Terrestrial Magnetism, Carnegie Institution of Washington, Washington D.C. 20015

<sup>12</sup>Johns Hopkins University and Space Telescope Science Institute, Baltimore, MD 21218

<sup>13</sup>University of Wisconsin, Madison, Wisconsin 53706

<sup>14</sup>Harvard Smithsonian Center for Astrophysics, Cambridge, MA 02138

<sup>15</sup>Royal Greenwich Observatory, Cambridge CB30EZ England

<sup>16</sup>Lick Observatory, University of California, Santa Cruz, CA 95064

<sup>17</sup>Infrared Processing and Analysis Center, Jet Propulsion Laboratory, California Institute of Technology, MS 100-22, Pasadena, CA 91125

## ABSTRACT

We report the discovery of Cepheid variable stars in the galaxy NGC 4414, as part of the *Hubble Space Telescope (HST)* Key Project on the Extragalactic Distance Scale. Observations were obtained with the *HST* Wide Field and Planetary Camera 2 (WFPC2) for 13 epochs at  $V$  (F555W) and 4 at  $I$  (F814W). Photometry was performed using two independent programs, DoPHOT and DAOPHOT/ALLFRAME. We find 11 Cepheids with high quality light curves and well determined periods of 19 to 70 days. Nine of these Cepheids are used in fitting the Period–Luminosity relation. Assuming a LMC distance modulus of 18.50 mag and  $E(B - V) = 0.10$  mag, we derive a reddening-corrected distance modulus for NGC 4414 of  $31.41 \pm 0.17$  (random)  $\pm 0.16$  (systematic) mag, corresponding to a distance of  $19.1 \pm 1.5$  (random)  $\pm 1.4$  (systematic) Mpc. We derive a mean color excess for NGC 4414 of  $E(V - I) = 0.02 \pm 0.05$  mag. NGC 4414 is a calibrator of the Tully-Fisher and Type Ia supernova secondary distance indicators, and we briefly discuss the implications of the new distance for these methods.

*Subject headings:* Cepheids – galaxies: distances and redshifts – galaxies: individual (NGC 4414)

## 1. Introduction

The goal of the *HST* Key Project on the Extragalactic Distance Scale is to measure  $H_0$  to an accuracy of 10%. Accurate distances to 18 nearby galaxies are being measured using Cepheid variable stars. These distances will be combined with *HST* Cepheid distances from other groups to calibrate several secondary distance indicators, including the Tully-Fisher (TF) relation, the surface brightness fluctuations method (SBF), the planetary nebula luminosity function (PNLF), the peak brightness of Type Ia supernovae, and the SN Type II expanding photosphere methods (EPM). A more complete description of the project can be found in Kennicutt, Freedman, & Mould (1995). Distances to M81, M101, M100, NGC 925, NGC 3621, NGC 3351, NGC 2090, NGC 7331 and NGC 1365 have already been determined (Freedman *et al.* 1994a, Kelson *et al.* 1996, Freedman *et al.* 1994b, Ferrarese *et al.* 1996, Silbermann *et al.* 1997, Rawson *et al.* 1997, Graham *et al.* 1997, Phelps *et al.* 1998, Hughes *et al.* 1998, and Madore *et al.* 1998, respectively).

NGC 4414 ( $\alpha_{2000} = 12^h26^m27.5^s$ ,  $\delta_{2000} = +31^\circ13'29''$ ) is host of the Type Ia supernova 1974G (Ciatti and Rosino 1977). It is an Sc(sr) II.2 galaxy (Sandage and Tammann 1981) seen at an inclination of  $56^\circ$  (Aaronson *et al.* 1982b) and is a calibrator for the Tully-Fisher relation. Previous distance estimates for NGC 4414 differ by as much as a factor two, from 10.5 Mpc (de Vaucouleurs 1975) to 18.2 Mpc (Pierce 1994). NGC 4414 is often assigned to the Coma I Cloud of galaxies (e.g. deVaucouleurs 1975, Sandage & Tammann 1975) though this assignment is questionable, and we will address this issue later. NGC 4414 has a heliocentric recessional velocity of  $720 \pm 11 \text{ km s}^{-1}$  (de Vaucouleurs *et al.* 1991) and lies near the triple valued region of Virgo supercluster inflow models (e.g. Aaronson *et al.* 1982a).

## 2. Observations and Data Reduction

### 2.1. Observing Strategy

Images of NGC 4414 were obtained with the *HST* WFPC2 camera. A detailed description of the instrument can be found in the WFPC2 Instrument Handbook (Biretta *et al.* 1996). The Wide Field Camera (WFC) images onto three  $800 \times 800$  CCD detectors, each with  $0''.10$  pixels and a  $1\frac{1}{3}$  field of view. The Planetary Camera (PC) makes use of a fourth CCD and has a  $34''$  field of view with  $0''.046$  pixels. All observations presented here were made with a gain setting of  $7\text{ e}^-/\text{DN}$  and at a CCD operating temperature of  $-88^\circ\text{ C}$ .

Figure 1 shows a ground-based *B* band image of NGC 4414 taken at the Fred Lawrence Whipple Observatory 1.2 meter telescope in  $\sim 2''.5$  seeing, with the footprint of WFPC2 overlain. A mosaic of the median images in all WFPC2 chips is shown in Figure 2. The small field was imaged by the Planetary Camera (PC); we refer to it throughout this paper as chip 1. We refer to the Wide Field Camera (WFC) fields as chips 2 through 4, in counter-clockwise direction from the PC, as projected on the sky.

A log of observations is given in Table 1. Twelve *V* (F555W), four *I* (F814W) and two *B* (F439W) epochs were obtained between April and June 1995 over a 62-day window. As with the other galaxies observed as part of the Key Project, the temporal sampling of the observations was chosen to produce more uniformly sampled light curves of potential Cepheids with periods between 5 and 60 days (Freedman *et al.* 1994a) and is illustrated in Figure 3. To facilitate cosmic ray (CR) removal and optimize the Cepheid-finding algorithms (see Section 4), each observation consisted of a pair of CR split images, for a total integration time of 2500 seconds in each filter. The *B* band images were found to have a low signal-to-noise ratio, and are not discussed further in this paper. An additional *V* epoch was obtained in April 1996, approximately one year after the end of the main

observing window, in order to constrain the periods of the longer–period Cepheids.

## 2.2. Data Reduction

All images were processed with the standard Space Telescope Science Institute (STScI) pipeline described by Holtzman *et al.* (1995a), using the most up-to-date calibration files available at the time the data were taken. Briefly, pipeline reduction includes correction of small analog-to-digital (A/D) errors, subtraction of a bias level image, subtraction of a superbias image, subtraction of a dark frame, and division by a flat field.

The data were then processed with standard team reduction steps as described in Ferrarese *et al.* (1996) and Stetson *et al.* (1998). Bad columns and pixels were masked with the data quality files produced by the pipeline. To correct for the geometric distortion in the WFPC2 cameras, images were multiplied by a pixel area map, normalized to the area of the median pixel in the image. This effect is not corrected by the standard pipeline flat fields, which conserve surface brightness, but not integrated fluxes. Vignetted areas of each chip were masked. Finally, all images were multiplied by 4 and converted to short integer to reduce disk space and allow for data compression. This gives an effective gain of  $1.75 \text{ e}^-/\text{DN}$  and a read noise of 4 DN. For a more detailed description of standard Key Project data reduction steps, see Ferrarese *et al.* (1996) and Stetson *et al.* (1998).

## 3. Photometric Reduction and Calibration

The compact size and high surface brightness of NGC 4414 make it one of the most challenging target fields in the Key Project sample (Figure 2). The bright stars are generally crowded and concentrated on the higher surface brightness areas of the galaxy. The background surface brightness of the galaxy has a steep gradient. In addition, the exposure

times are relatively short for a target at the distance of NGC 4414. The center of the galaxy is located in the PC field, and crowding problems are especially severe, compromising the photometric accuracy of the data in this field. Only one high quality Cepheid (C12 in Appendix B) was found in the PC field, and it lies near the optical pyramid edge of the chip where the photometry may be unreliable. Therefore, we use only the Cepheids found in the WFC fields to calculate the distance to NGC 4414.

The effect of crowding on the photometry of stars in these galaxies is a serious issue. To address this, our team has performed a series of artificial star tests (Ferrarese *et al.* 1998). We find that the crowding effects on the stellar photometry in regions such as those in which our Cepheids are found is negligible, although stars in more crowded region may indeed be affected. Normal precautions were taken to avoid contaminated Cepheid photometry, including examining images for nearby companions, and checking the color of the Cepheid and the amplitude of its lightcurve.

Photometry was performed on the WFPC2 images through two parallel and independent reduction tracks, each using a separate photometry program, ALLFRAME/DAOPHOT II (Stetson 1994) and a variant of DoPHOT optimized for undersampled *HST* WFPC2 images (Saha *et al.* 1996). Each reduction is described separately below.

### 3.1. ALLFRAME/DAOPHOT Reductions

To extract accurate photometry from all images, a complete star list was constructed as follows. All available images from each chip were median combined to produce a deep, clean, CR free image. DAOPHOT and ALLSTAR (Stetson 1987) were used to find stars, add them to the star list, and subtract them from the median image to uncover other stars on the image. After a few DAOPHOT/ALLSTAR iterations, the remaining stars visible on

the image were added to the list by hand. ALLFRAME (Stetson 1994) was then run on all images using this initial star list. All star-subtracted images produced by ALLFRAME were again median combined and examined. Star-subtracted  $V$  and  $I$  images were also separated by filter and median combined to locate any extremely blue or red stars. Any remaining stars on these images were added to the final star list. The point spread functions (PSFs) created for WFPC2 images from public domain images of the globular clusters Pal 4 and NGC 2419 (Hill *et al.* 1998) were used by ALLFRAME to extract photometry for all stars on the final star list. Variations in PSF due to telescope guiding and focus changes are accounted for by applying a separate aperture correction to each frame.

ALLFRAME instrumental magnitudes were converted to standard Johnson  $V$  and Cousins  $I$  as described in Hill *et al.* (1998). Aperture corrections which convert the instrumental PSF fit magnitudes to 0".5 aperture magnitudes were calculated with the program DAOGROW (Stetson 1990), using observations of bright isolated stars in NGC 4414, along with observations of several globular clusters and Key Project galaxies, including NGC 2419, Pal 3, Pal 4, M101, NGC 925, NGC 1365, NGC 3621, NGC 4725, and NGC 7331. The larger data set was used to derive the general form of the growth curves, while the NGC 4414 data provided proper correction for core broadening due to small focus variations and spacecraft jitter for each epoch. This procedure makes maximum use of the full library of isolated star observations to define the gross form of the growth curves, while accurately correcting for image shape variation in each individual observation. For details see Stetson *et al.* (1998). A separate aperture correction was calculated for each chip-filter combination at each epoch. Average aperture corrections for each chip-filter combination are listed in Table 2. We use the team-standard long exposure zero points from Table 7 of Hill *et al.* (1998), also listed in Table 2. The conversion equations used to transform ALLFRAME instrumental magnitudes to the standard system are of the form

$$M = m + 2.5 \log t + A1 + A2 * (V - I) + A3 * (V - I)^2 \quad (1)$$

where  $M$  is the standard magnitude,  $m$  is the instrumental magnitude,  $t$  is the exposure time, and  $A1$  through  $A3$  are constants.  $A2$  and  $A3$  are taken directly from Holtzman *et al.* (1995a).  $A1$  accounts for the adopted zero point, aperture corrections, the normalization of our pixel area map, a factor of  $2.5 \log 4$  from our conversion to short integer, and the ALLFRAME zero point of 25 mag. Explicitly,

$$A1 = ZP + AC + 0.016 + 2.5 \log 4 - 25. \quad (2)$$

$A1$ ,  $A2$ , and  $A3$  are listed in Table 2 for each chip and filter combination.

### 3.2. DoPHOT Reductions

DoPHOT reductions followed the process outlined in Ferrarese *et al.* (1996). To summarize, a master list of stars was compiled by running DoPHOT on deep  $V$  and  $I$  images made by co-adding all F555W and F814W frames, and removing cosmic rays according to the procedure in Saha *et al.* (1996). DoPHOT was then run on the resulting 12  $V$  and 4  $I$  images, using the master star list as input. Aperture corrections were derived from observations of the Leo I dwarf galaxy (where the field was relatively uncrowded), with the offset to NGC 4414 derived from the deep  $V$  and  $I$  images of NGC 4414 itself. Data from the globular cluster, Pal 4, were then used to put the resulting magnitudes on the system of Holtzman *et al.* (1995a).

### 3.3. Comparison of ALLFRAME/DoPHOT Photometry

DoPHOT reductions were completed before the 1996 revisit data were available, so all comparisons presented here are limited to the first 12 epochs of NGC 4414 data. A comparison of ALLFRAME and DoPHOT photometry for the local standards is shown in Figure 4 and summarized in Table 3. The agreement of the photometry for the local

standards (crosses) is very good for all the WFC fields, considering the severe crowding, with the largest difference of about 0.06 mag in  $I$  in chip 4 and average differences (ALLFRAME–DoPHOT) for all three chips of  $-0.020 \pm 0.008$  mag in  $V$  and  $+0.064 \pm 0.008$  mag in  $I$ .

The comparison of ALLFRAME and DoPHOT intensity-averaged magnitudes (described explicitly in Section 5) for each of the Cepheid candidates is plotted in Figure 4 as solid circles. The mean difference is  $+0.04 \pm 0.03$  mag in  $V$  for chips 2 through 4, and  $+0.03 \pm 0.04$  in  $I$ . The Cepheids are typically fainter than the local standards, and as expected the scatter in the comparison is larger, but it is clear that the Cepheids tend to lie within the error envelope defined by the standard stars.

#### 4. Identification of Variable Stars

Variable stars were identified following the procedures described in previous papers in this series. However, because of the unusual level of stellar crowding in this galaxy, several different variable finding tests were employed in order to maximize the number of variable star candidates. The light curves of all candidates were rigorously checked in both photometry sets. Only those stars which were independently confirmed in both photometry sets were included in the final sample.

Three separate variable finding tests were used with the ALLFRAME data set. The first method simply looked for stars with unusually high dispersion in their  $V$  magnitudes. The second method used a correlated variability test suggested by Welch & Stetson (1993), which takes advantage of the CR split data, since real variables will have a similar change in magnitude from epoch to epoch in both of its CR split images; random noise and CR hits will not be correlated in the CR split images, on average. The periods of the variable

candidates were determined using a phase dispersion minimization routine as described by Stellingwerf (1978) and detailed in Freedman (1994a). The third variable finding method, described by Stetson (1996), also finds variable candidates using a variation of the Welch & Stetson (1993) technique, but finds periods, mean magnitudes, and amplitudes by fitting template light curves.

The DoPHOT photometry was searched independently for variables, following the procedures of Saha & Hoessel (1990) and Ferrarese *et al.* (1996). A chi-squared test was used, and stars that had a 99% confidence of being variable were checked for periodicity using a variant of the Lafler & Kinman (1965) method of phase dispersion minimization.

As expected for our sampling strategy (see Figure 2), period aliasing was not a problem for the 11 Cepheids in our sample. Light curves were examined for possible alternate periods and these were ruled out. The one year revisit data also helped to constrain periods, especially for some of the longer period Cepheids.

The final Cepheid sample was compiled from these lists of variable candidates. In cases where a promising candidate was initially discovered in only one photometry set, it was extracted by hand from the second. If the second light curve was convincing and consistent with the first, it was also added to the variable star lists. The light curve from each potential variable was examined and candidates were confirmed on the basis of light curve shape, amplitude, and consistency between the two photometry sets. The images were visually examined to ensure variability, and to confirm that candidates were not in extremely crowded regions. The images were blinked visually as a final check. Our final sample includes 11 Cepheid candidates, 9 of which we use to fit the period-luminosity (PL) relation.

Finder charts for the Cepheid candidates are shown in Figures 5 and 6. Figure 5 shows the PC chip and each of the three WFC chips with the locations of the Cepheid fields

indicated. Figure 6 shows small  $51 \times 51$  pixels fields centered on each Cepheid candidate, corresponding to a  $5''$  field of view. In addition to these Cepheid candidates, there were 10 variable candidates that were not retained in our final list. These possible Cepheids are also marked in Figure 5 and are described in more detail in Appendix B.

## 5. Light Curves and Cepheid Parameters

Since the ALLFRAME photometry set includes the revisit data, all periods and mean magnitudes presented here are based on the ALLFRAME photometry. In all cases, the DoPHOT photometry is consistent with the periods and magnitudes presented (the DoPHOT-based analysis is summarized in the next section). The magnitudes for the CR split pair within each epoch were averaged and CR contaminated photometry rejected. The resulting  $V$  and  $I$  photometry for each epoch is given in Tables 4 and 5. The uncertainties in instrumental magnitudes reported by ALLFRAME, based on photon statistics and quality of PSF fit, are also given. Light-curves for the Cepheid candidates are plotted in Figure 7.

As with other Key Project galaxies, both an intensity-averaged magnitude

$$m = -2.5 \log \sum_{i=1}^n \frac{1}{n} 10^{-0.4 \times m_i}, \quad (3)$$

and a phase-weighted mean magnitude

$$m = -2.5 \log \sum_{i=1}^n 0.5 (\phi_{i+1} - \phi_{i-1}) 10^{-0.4 \times m_i}, \quad (4)$$

were calculated, where  $n$  is the total number of observations, and  $m_i$  and  $\phi_i$  are the magnitude and phase of the  $i$ th observation in order of increasing phase. For variables with uniformly sampled light curves, these two magnitudes coincide. For our sample of Cepheids, the difference between phase weighted mean magnitudes and intensity-averaged magnitudes is  $0.034 \pm 0.027$  at  $V$  and  $0.024 \pm 0.014$  at  $I$ , in the sense that phase-weighted

mean magnitudes are slightly fainter. The choice of phase-weighted or intensity-averaged magnitudes will be shown not to affect the distance modulus to NGC 4414 significantly.

Only four epochs were observed at  $I$ , and the poor phase coverage makes both the intensity-averaged and phase-weighted magnitudes poor representations of the  $I$  mean magnitude. Freedman (1988) showed that Cepheids have very good correspondence between  $V$  and  $I$  light curves, and that the ratio of the  $V$  to  $I$  amplitude is 1:0.51. We therefore correct the  $I$  mean magnitudes in the following way. We calculate the mean  $V$  magnitude at only those epochs where  $I$  observations were also made. The difference in the 13-epoch and 4-epoch  $V$  magnitudes is multiplied by the  $I$  to  $V$  Cepheid amplitude ratio, and then added to the  $I$  magnitude, averaged over four epochs. This yields the corrected mean  $I$  magnitude. Because the light curves are well sampled in almost all cases, corrections for NGC 4414 were typically very small, about  $\pm 0.05$  mag, with an average of  $-0.036 \pm 0.023$  mag, and a maximum correction of  $-0.17$  mag.

For each Cepheid candidate, Table 6 presents the chip number, equatorial coordinates, period, intensity-averaged and phase-weighted mean  $V$  and  $I$  magnitudes and errors, the  $I$  band correction described above (labeled  $I - I_4$ ), and a description. Uncertainties in the mean magnitudes are calculated by propagating the instrumental uncertainties for the photometry of each epoch through Equation 3 or 4, as appropriate. Figure 8 shows an  $I$  versus  $V - I$  color magnitude diagram (CMD) of all the stars on chips 2 through 4 with the Cepheid candidates over plotted as solid circles. The CMD lacks the well defined main sequence and red supergiant plume that are seen in more nearby and less crowded galaxies like M81 (Hughes *et al.* 1994) and NGC 925 (Silbermann *et al.* 1996). This is undoubtedly a result of the extreme crowding in NGC 4414. Most of the Cepheid candidates lie in the area of the instability strip.

Two of the Cepheid candidates were excluded from the PL fit for the following reasons.

Images are still spherically aberrated when they intersect the pyramid mirror, so all stars within roughly  $1''.25$  of the edge of any chip have their light split between two chips. Cepheid candidate C9 was excluded from the fit to the PL relation because it lies near the pyramid edge of chip 4, and up to 18% of its light may be lost. Candidate C6 was also checked for this effect, but was found to lose  $< 1\%$  of its light, so it was retained in the PL fit. We have retained candidate C4 in the final Cepheid sample because of its classic Cepheid light curve at  $V$ , but have excluded it in fitting the PL relation due to its unusually red color,  $V - I = 1.60$  in the ALLFRAME phase-weighted photometry.

## 6. Period Luminosity Relations and the Distance to NGC 4414

The method used to determine the distance to NGC 4414 is the same as that used in other papers of the Key Project series. A more detailed description of this method is given in Ferrarese *et al.* (1996). Only a brief summary will be provided here.

The apparent  $V$  and  $I$  distance moduli to NGC 4414 were derived using the standard  $V$  and  $I$  PL relations listed by Madore & Freedman (1991), based on LMC Cepheid data, scaled to a true modulus of 18.50 mag and corrected for an average LMC reddening of  $E(B - V) = 0.10$  mag. The adopted PL relations are

$$M_V = -2.76 (\log P - 1.0) - 4.16 \quad (5)$$

and

$$M_I = -3.06 (\log P - 1.0) - 4.87 \quad (6)$$

These are the same PL relations used in Saha *et al.* (1997) and other papers in that series.

The slope of the PL relations was fixed to those of the LMC in the fit to the NGC 4414 Cepheid data. By solving for only the zero point in the regression, we avoid bias in the slope due to incompleteness at faint magnitudes.

The  $V$  and  $I$  phase-weighted PL relations for NGC 4414 are shown in Figure 9. Open circles are Cepheid candidates which were not used in the fit for reasons discussed in the previous section. The solid lines represent the best fit to the LMC PL relations, while the dotted lines show two sigma deviations from the mean LMC PL relations, at  $\pm 0.54$  mag for  $V$  and  $\pm 0.36$  mag for  $I$  (Madore & Freedman 1991). Given the width of the instability strip, almost all Cepheids will fall inside these limits, in the absence of differential reddening. These PL relations give apparent distance moduli of  $\mu_V = 31.45 \pm 0.13$  mag and  $\mu_I = 31.43 \pm 0.09$  mag, where the quoted errors are calculated from the scatter in the NGC 4414 PL relations.

Much of the scatter in the  $V$  and  $I$  PL relations is correlated between the bandpasses, due to the effects of differential reddening and position within the finite width of the instability strip. Figure 10 shows a plot of the  $I$ -band PL residuals versus the  $V$ -band residuals for the NGC 4414 Cepheids. The solid line shows the slope and full width of the expected correlation due to intrinsic instability strip width. The dotted line shows the effect of differential reddening. There is good agreement between the data and both the expected width and slope of the residual correlations. Uncorrelated photometric errors of approximately 0.09 mag, divided between the  $V$  and  $I$  photometry are the most likely source of the remaining scatter shown in Figure 10.

To derive the true distance modulus for NGC 4414, we must correct for the average line-of-sight reddening to the Cepheids. The true distance modulus  $\mu_0$ , defined as

$$\mu_0 = \mu_V - A_V = \mu_I - A_I, \quad (7)$$

requires that

$$\mu_V - \mu_I = A_V - A_I = E(V - I). \quad (8)$$

For our sample of Cepheids, we find  $E(V - I) = 0.02 \pm 0.05$  mag. The Cardelli *et al.* (1989)

extinction law gives

$$A(I)/A(V) = 0.773 - 0.587/R_V \quad (9)$$

for the Johnson  $V$  and Cousins  $I$  passbands with  $R_V = A(V)/E(B - V)$ . We assume  $R_V = R_V^{\text{LMC}} = 3.30$  as in previous papers in the series, e.g. Ferrarese *et al.* (1996). This gives a true distance modulus to NGC 4414 of  $\mu_0 = 31.41 \pm 0.09$  mag, corresponding to a distance of  $19.1 \pm 0.8$  Mpc.

The choice of photometry set or method for finding Cepheid mean magnitudes does not affect our derived distance modulus. Distance moduli derived from ALLFRAME and DoPHOT intensity-averaged and phase-weighted magnitudes are given in Table 7. The effects of excluding the most deviant point in the sample (C6), as well as including all Cepheid candidates, are also shown. Each of these moduli is consistent within the errors with the modulus derived from ALLFRAME phase-weighted magnitudes above.

The errors cited above are all internal errors, arising from the scatter in the NGC 4414 PL relations. To get a more realistic estimate in the uncertainty in the distance, we must consider other possible random or systematic errors in the Cepheid PL fitting method. Table 8 presents the error budget for the distance to NGC 4414. We include the uncertainties due to metallicity, LMC distance modulus, and photometric calibration, in addition to the uncertainty arising from the scatter of the PL relations, correlated between the  $V$  and  $I$  bandpasses. Errors are classified as either “random” or “systematic” as described in Phelps *et al.* (1998).

A potential source of systematic error in the distance to NGC 4414 is the possible metallicity dependence of the Cepheid PL relation at  $V$  and  $I$ . Kennicutt *et al.* (1997) have analyzed *HST* photometry of two Cepheid fields in M101, and find weak evidence for a metallicity dependence, at the level of  $d(m - M)_0/d[O/H] = -0.24 \pm 0.16$  mag/dex. If the average abundance of the NGC 4414 Cepheids differs substantially from that of the LMC

Cepheids which calibrate the PL relation, this could introduce a small but significant error in the derived distance.

Unfortunately there are no published H II region abundances available for this galaxy, so we can only estimate the abundance of the Cepheid field, using the relation between absolute magnitude and abundance of Zaritsky, Kennicutt, & Huchra (1994). Combining the distance measured in this paper with photometry from Tully (1988) yields  $M_B = -20.3$  mag for NGC 4414. The mean H II region abundance of Sc galaxies in the Zaritsky *et al.* (1994) sample is  $\log(O/H) = -3.1$ , or approximately solar, measured at the average radius of the Cepheids ( $\rho/\rho_0 = 0.6$ ). This crude estimate is uncertain by at least a factor of two, due to the dispersion in the metallicity-luminosity relation. Thus the NGC 4414 Cepheids are likely to be  $\sim 2$  times more metal-rich than the LMC Cepheids, which could cause the Cepheid distance of NGC 4414 to be underestimated by a few hundredths to several hundredths of a magnitude. Given the uncertainties in these estimates, we have not attempted to apply a metallicity correction, and instead include the uncertainty in the error budget in Table 8. We plan to measure H II abundances for this galaxy, and will revisit this question at the conclusion of the Key Project.

## 7. Comparison to Previous Distance Estimates

Previous distance estimates to NGC 4414 have been either based on measurements of NGC 4414 itself, or on indirect estimates via its assumed membership in the Coma I Cloud. Table 9 compares our measurement to previous distance estimates for NGC 4414. Most of the recent measurements to NGC 4414, based on either the TF method or the peak brightness of SN 1974G, lie in the 17-18 Mpc range, in excellent agreement with our value of  $19.1 \pm 1.5 \pm 1.4$  Mpc.

As mentioned earlier, the distribution of galaxies in the Coma I region appears to be much more complex than originally assumed. The Coma I Cloud is the classical deVaucouleurs (1975) group 13, and the Coma-Sculptor cloud of Tully (1988). It is a loose group, spread over more than  $10^\circ$ , with a core of ellipticals. Aaronson & Mould (1983) examined the TF relation for the Coma I group, and found an unusually large dispersion. The CfA2 redshift survey shows only a loose association of galaxies around NGC 4414, perhaps two groups slightly offset in right ascension centered around  $12^h20^m$  and  $700 \text{ km s}^{-1}$  and  $12^h15^m$  and  $1000 \text{ km s}^{-1}$  (Huchra & Geller 1997). The Virgo-centric flow model (Aaronson *et al.* 1982a) is unhelpful, because NGC 4414 is  $18^\circ$  away from the center of the Virgo cluster and in the “triple-value zone,” where distance is not a single valued function of redshift. Distances determined for some other members of Coma I by the PNLf, GCLF, and SBF methods are significantly lower than that derived for NGC 4414 (Jacoby *et al.* 1996, Flemming *et al.* 1995, Simard & Pritchett 1994, respectively). However, a recent determination of the distance to the Coma I Cloud using SBF distances to 3 galaxies yields a distance of 15.5 Mpc (Tonry *et al.* 1997). Taken together, these results suggest the Coma I Cloud probably is not a distinct group, and more likely is a projection of galaxies along the line of sight, or perhaps two superposed groups. Our distance to NGC 4414 is therefore of limited use for calibrating secondary distance indicators pertaining to the Coma I Cloud.

## 8. Implications for Secondary Distance Indicators

Because of the proximity of NGC 4414 to the Virgo cluster, its peculiar velocity correction is highly uncertain and model-dependent. Hence any value of  $H_0$  calculated from the distance and radial velocity of this galaxy alone is virtually meaningless. However, NGC 4414 adds important calibration points for both the TF relation and the SN Ia peak brightness methods. More complete discussions of the impact of the Key Project distances

on these calibrations will be presented in the future. Here, we briefly discuss the consistency of the NGC 4414 results with existing calibrations.

In Figure 11, calibrators of the TF relation are plotted (Mould *et al.* 1995 and references therein). This sample includes both galaxies with direct Cepheid distance measurements and galaxies included from group associations. We use our new Cepheid distance modulus and  $H_{-0.5}^c = 7.83$  mag and  $\Delta V_{20}^c = 509$  km s<sup>-1</sup> from Aaronson *et al.* (1982b) to place NGC 4414 on this plot, shown as an open circle with error bars. The overplotted line is the calibration of Mould *et al.* (1995). The new Cepheid distance to NGC 4414 places it approximately 0.3 mag above this line, well within the observed scatter of 0.5 mag.

NGC 4414 was host to a Type Ia SN, 1974G. Photographic photometry published by Ciatti & Rosino (1977) and subsequently reanalyzed by Leibundgut *et al.* (1991) and Vaughan *et al.* (1995) are shown in Table 10, along with the reddening corrected values, and the  $M_B$  and  $M_V$  magnitudes of SN 1974G derived using our new distance to NGC 4414. The reddening corrections to the observed values are quite uncertain, given the large uncertainty in the observed color and in the assumed intrinsic  $(B - V)_{B_{max}}$  for the supernova. The absolute magnitudes of SN 1974G are in reasonable agreement with the average SN Type Ia luminosities as determined by Saha *et al.* (1997),  $M_{B_{max}}^0 = -19.52 \pm 0.07$  mag and  $M_{V_{max}}^0 = -19.48 \pm 0.07$  mag. For comparison, the calibration of Hamuy *et al.* (1996) gives  $M_{B_{max}}^0 = -19.26 \pm 0.05$  mag, and  $M_{V_{max}}^0 = -19.27 \pm 0.05$  mag for  $\Delta m_{15}(B) = 1.1$  mag, which is consistent with the  $\Delta m_{15}(B)$  of the light curve of SN 1974G (Leibundgut *et al.* 1991). The photometry of SN 1974G was recalibrated with photoelectric measurements of its standard sequences by Tsvetkov (1986) as reported by Patat *et al.* (1997). This new photometry plus our distance modulus gives  $M_{B_{max}}^0 = -20.33 \pm 0.84$ , as shown in Table 10. Like previous photometry, the large error is due to a large uncertainty in the reddening correction to the supernova. It is clear that the usefulness of SN 1974G as a calibrator of

the SN Type Ia secondary distance indicator is limited by the quality of the photometry of the supernova, and not by our derived distance to NGC 4414.

The work presented in this paper is based on observations with the NASA/ESA Hubble Space Telescope, obtained by the Space Telescope Science Institute, which is operated by AURA, Inc. under NASA contract No. 5-26555. Support for this work was provided by NASA through grant GO-2227-87A. This research has made use of the NASA/IPAC Extragalactic Database (NED) which is operated by the Jet Propulsion Laboratory, Caltech, under contract with the National Aeronautics and Space Administration. PBS and SMGH are grateful to NATO for travel support via a Collaborative Research Grant (960178). LF acknowledges support from NASA through Hubble Fellowship grant #HF-01081.01-96A, awarded by the Space Telescope Science Institute. AT gratefully acknowledges partial support from an NSF graduate fellowship.

### **Appendix A: Secondary Standards**

Several relatively isolated stars were chosen on each WFC chip to serve as local standards. In addition to their isolation, these stars were picked because their profiles were well fit by ALLFRAME, photometric errors were small with good frame-to-frame repeatability, their sky background was uncomplicated, and they were relatively bright. The  $V$  and  $I$  magnitudes of these stars derived from their ALLFRAME photometry are given in Tables 11a–c.

### **Appendix B: Other Possible Variable Stars**

Several variable candidates were excluded from the list of Cepheid candidates, due to the shapes of their light curves, low amplitude, inconsistency between photometry sets,

degree of crowding, or location on the PC. Those candidates which appear to have real variability are listed in Table 12 along with their chip number, coordinates, possible period, and intensity-averaged  $V$  and  $I$  magnitudes. Finder charts are given in Figure 12.

## REFERENCES

- Aaronson, M., Huchra, J., Mould, J., Schechter, P.L., & Tully, R. B. 1982a, ApJ, 258, 64.
- Aaronson, M., *et al.* , 1982b, ApJS, 50, 241
- Aaronson, M., & Mould, J. 1983, ApJ, 265, 1
- Biretta, J. A., *et al.* 1996, WFPC2 Instrument Handbook, Version 4.0 (Baltimore: STScI)
- Cardelli, J.A., Clayton, G.C., & Mathis, J.S. 1989, ApJ, 345, 245
- Ciatti, F. & Rosino, L. 1977, A&A, 57, 73
- deVaucouleurs, G. 1975, in *Galaxies and the Universe (Stars and Stellar Systems X)* eds. Sandage, Sandage, & Kristian, U. Chicago Press, p. 577
- deVaucouleurs, G. 1979, ApJ, 227, 729
- deVaucouleurs, G. *et al.* 1991, *Third Reference Catalog of Bright Galaxies*, (New York: Springer-Verlag)
- Ferrarese, L. *et al.* 1996, ApJ, 464, 568
- Ferrarese, L. *et al.* 1998, in prep
- Flemming, D.E.B., Harris, W.E., Pritchett, C.J., & Hanes, D. A. 1995, AJ, 109, 1044
- Freedman, W. L., 1988, ApJ, 306, 691
- Freedman, W.L. *et al.* 1994a, ApJ, 427, 628
- Freedman, W.L. *et al.* 1994b, Nature, 371, 757
- Graham, J. A. *et al.* 1997, ApJ, 477, 535
- Hamuy, M., Phillips, M.M., Schommer, R.A., & Suntzeff, N.B. 1996, AJ, 112, 2391
- Hill, R. *et al.* 1998, ApJ, in press
- Höflich, P. & Khokhlov, A. 1996, ApJ, 457, 500

- Holtzman, J.A. *et al.* 1995a, PASP, 107, 156
- Holtzman, J.A. *et al.* 1995b, PASP, 107, 1065
- Huchra, J.P. & Geller, M.J. 1997, private communication
- Hughes, S.M.G. *et al.* 1994, ApJ, 428, 143
- Hughes, S.M.G. *et al.* 1998, ApJ, submitted
- Kelson, D. *et al.* 1996, ApJ, 463, 26
- Kennicutt, R.C., Freedman, W.L., & Mould, J.R. 1994, AJ, 110, 1476
- Kennicutt, R.C. *et al.* 1997, in press
- Jacoby, G.H., Ciardullo, R., & Harris, W.E. 1996, ApJ, 462, 1
- Lafler, J., & Kinman, T.D. 1965, ApJS, 11, 216
- Leibundgut, B., Tammann, G.A., Cadonau, R., & Cerrito, D. 1991, A&AS, 89, 537
- Madore, B.F., & Freedman, W.L. 1991, PASP, 103, 933
- Madore, B.F. *et al.* 1998, Nature, submitted
- Mould, J. *et al.* 1995, ApJ, 449, 413
- Müller, E. & Höflich, P. 1994, A&A, 281, 51
- Patat, E., Barbon, R., Cappellaro, E., & Turatto, M. 1997, A&A, 317, 423
- Phelps, R. *et al.* 1998, ApJ, in press
- Pierce, M.J. 1994, ApJ, 430, 53
- Rawson, D.M. *et al.* 1997, ApJ, 490, 517
- Saha, A., & Hoessel, J.G. 1990, AJ, 99, 97
- Saha, A. *et al.* 1996, ApJ, 466, 55
- Saha, A. *et al.* 1997, ApJ, 486, 1

- Sandage, A., & Tammann, G. 1975, *ApJ*, 196, 313
- Sandage, A., & Tammann, G. 1981, in *A Revised Shapley-Ames Catalogue of Bright Galaxies*, Carnegie Institution of Washington, Washington DC
- Schaefer, B. E. 1995, *ApJ*, 450, L5
- Silbermann, N.A. *et al.* 1996, *ApJ*, 470, 1
- Simard, L. & Pritchett, C.J. 1994, *AJ*, 107, 503
- Stellingwerf, R.F. 1978, *ApJ*, 224, 953
- Stetson, P.B. 1987, *PASP*, 99, 191
- Stetson, P.B. 1990, *PASP*, 102, 932
- Stetson, P.B. 1994, *AJ*, 106, 205
- Stetson, P.B. 1996, *PASP*, 108, 851
- Stetson, P.B. *et al.* 1998, in prep
- Tonry, J.L., Blakeslee, J.B., Ajhar, E.A., & Dressler, A. 1997, *ApJ*, 475, 399
- Tsvetkov, D., Yu. 1986, *Peremmenye Zvezdy*, 22, 279
- Tully, R. B., 1988, *Nearby Galaxies Catalog* (Cambridge: Cambridge University Press)
- Vaughan, T.E., Branch, D., Miller, D.L., & Perlmutter, S. 1995, *ApJ*, 439, 558
- Welch, D.L., & Stetson, P.B. 1993, *AJ*, 105, 1813
- Westerlund, B.E. “The Magellanic Clouds”, Cambridge University Press, 1997, Section 2.7
- Zaritsky, D., Kennicutt, R. C. , & Huchra, J.P. 1994, *ApJ*, 420, 87

Fig. 1.— *B*-band image of NGC 4414 taken at the FLWO 1.2m telescope in  $\sim 2''.5$  seeing. Superimposed is the *HST*/WFPC2 field of view.

Fig. 2.— A mosaic of the median WFPC2 images of NGC 4414. Both *V* and *I* images were included. Scaling is logarithmic to show detail. North is toward the top, and east to the left.

Fig. 3.— Sampling variance of light curves for data taken using the temporal sampling of the NGC 4414 observations. The variance plotted is a measure of the degree to which the observed phase sampling deviates from that of uniform phase sampling. The variance is normalized such that zero variance corresponds to the case where the light curve is uniformly sampled.

Fig. 4.— Comparison of ALLFRAME and DoPHOT intensity-averaged magnitudes for secondary standard stars and Cepheid candidates located on chips 2 through 4. Standard stars from Table 3 are represented by crosses and Cepheid candidates by solid circles.

Fig. 5a.— The PC field of view in NGC 4414. Marked are the locations of the variable candidates' fields shown in detail in Figure 12. North is toward the bottom, and east to the right.

Fig. 5b.— The WFC2 field of view in NGC 4414. Marked are the locations of the variable candidates' fields shown in detail in Figures 6 and 12. North is toward the left, and east to the bottom.

Fig. 5c.— The WFC3 field of view in NGC 4414. Marked are the locations of the variable candidates' fields shown in detail in Figures 6 and 12. North is toward the top, and east to the left.

Fig. 5d.— The WFC4 field of view in NGC 4414. Marked are the locations of the variable candidates' fields shown in detail in Figures 6 and 12. North is toward the right, and east

to the top.

Fig. 6a.— Finder charts for each of the Cepheid candidates. Each image is  $51 \times 51$  pixels, corresponding to  $5''$ . Orientation of each image is as in Figure 5.

Fig. 6b.— Finder charts for each of the Cepheid candidates. Each image is  $51 \times 51$  pixels, corresponding to  $5''$ . Orientation of each image is as in Figure 5.

Fig. 7a.— Light curves for each of the 11 Cepheid candidates. The  $V$  magnitudes are plotted as solid squares, and  $I$  as open triangles. Data are plotted over a second cycle for clarity.

Fig. 7b.— Light curves for each of the 11 Cepheid candidates. The  $V$  magnitudes are plotted as solid squares, and  $I$  as open triangles. Data are plotted over a second cycle for clarity.

Fig. 8.—  $I$  vs.  $V - I$  color-magnitude diagram for the 3 WFC chips. Phase weighted  $I$  magnitude and color are plotted for each of the Cepheid candidates as solid circles.

Fig. 9.— The  $V$  and  $I$  PL relations for the Cepheids listed in Table 6. The solid line represents the best fit to the NGC 4414 data. The dotted lines represent the scatter expected due to the intrinsic width of the Cepheid instability strip. Cepheid candidates excluded from the fit are plotted as open circles.

Fig. 10.— Magnitude residuals in  $I$  and  $V$  from the PL relations for Cepheids in NGC 4414. Cepheids excluded from the fit are represented as open circles. The expected scatter due to the intrinsic width of the instability strip is represented by the solid line. The correlation expected due to differential reddening is given by the dotted line. The dashed line is a fit to the data.

Fig. 11.— The  $H$  band Tully-Fisher relation. Local calibrators from Mould *et al.* (1995) and references therein are plotted as solid circles. NGC 4414 is placed on this plot using the data of Aaronson *et al.* (1982b) and our new distance modulus, and is represented as

an open circle with error bars. The line is the  $H$  band TF calibration given by Mould *et al.* (1995).

Fig. 12a.— Finder charts for the additional variable candidates. Each image is  $51 \times 51$  pixels, corresponding to  $5''$  for the WFC and  $2''.5$  for the PC (candidates C12, C14, and C15). Orientation of each image is as in Figure 5.

Fig. 12b.— Finder charts for the additional variable candidates. Each image is  $51 \times 51$  pixels, corresponding to  $5''$ . Orientation of each image is as in Figure 5.

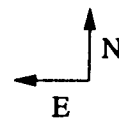
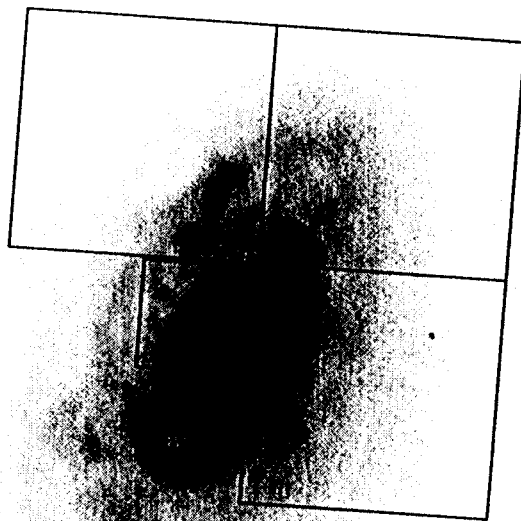


Fig. 1.— *B*-band image of NGC 4414 taken at the FLWO 1.2m telescope in  $\sim 2''.5$  seeing. Superimposed is the *HST*/WFPC2 field of view.

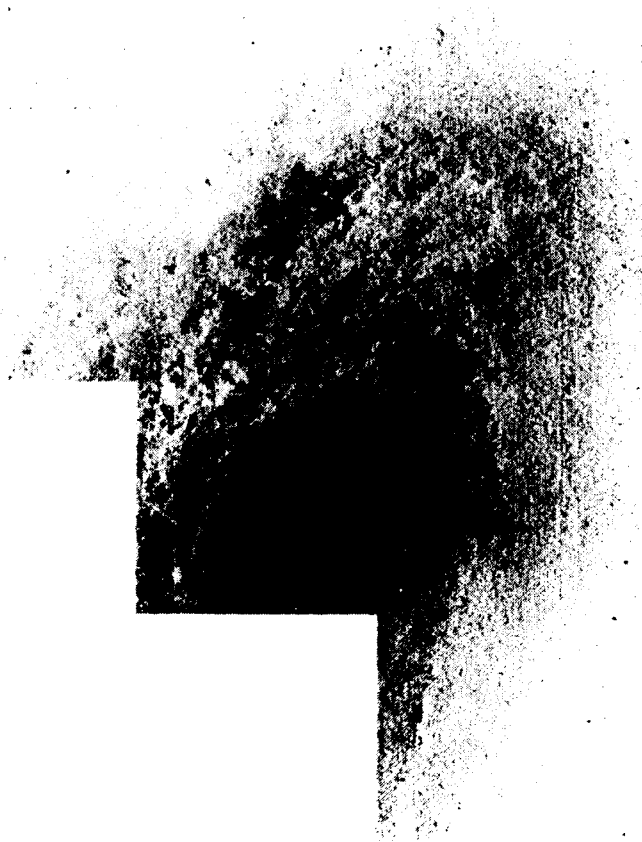


Fig. 2.— A mosaic of the median WFPC2 images of NGC 4114. Both  $V$  and  $I$  images were included. Scaling is logarithmic to show detail. North is toward the top, and east to the left.

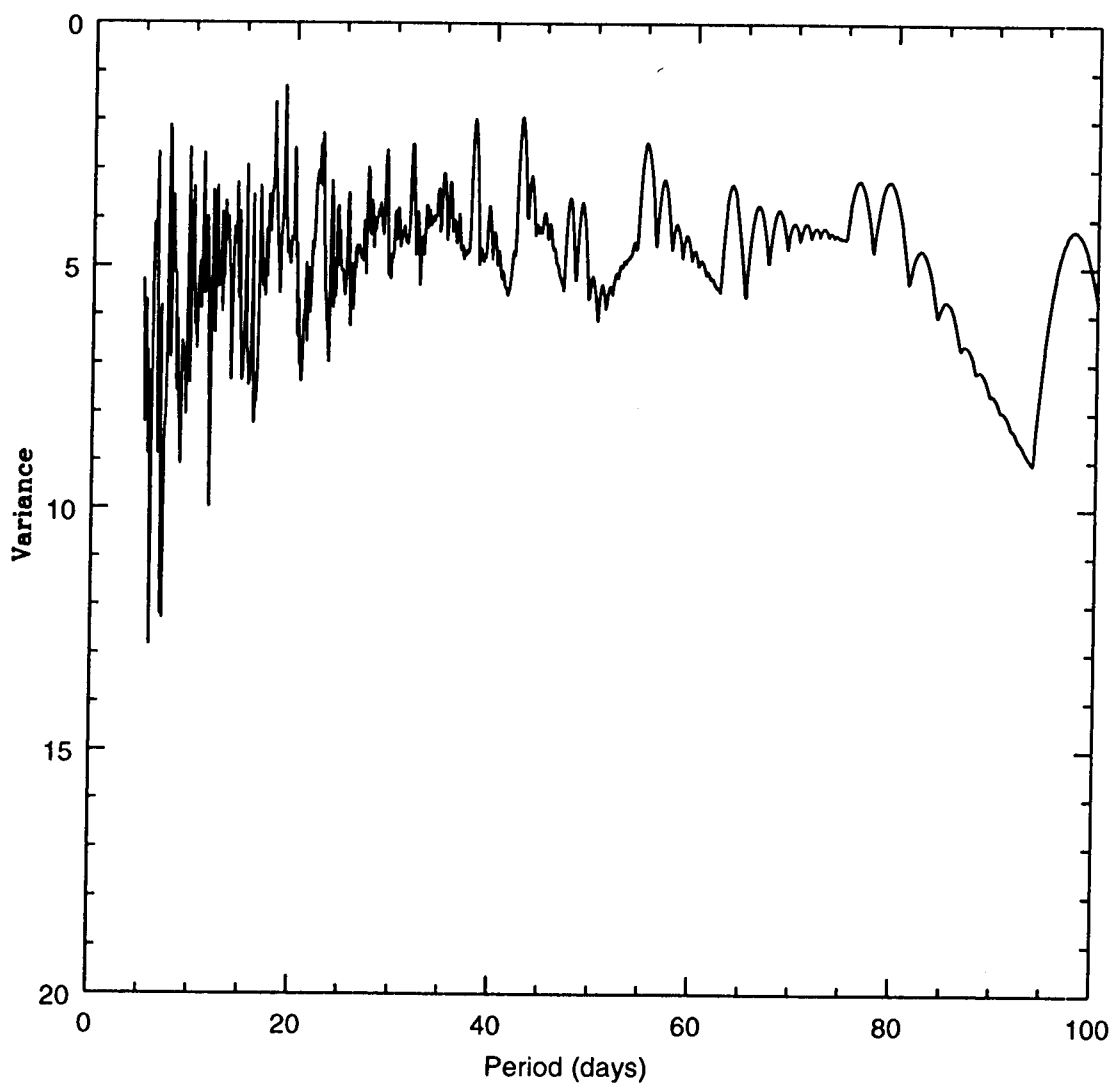


Fig. 3.— Sampling variance of light curves for data taken using the temporal sampling of the NGC 4414 observations. The variance plotted is a measure of the degree to which the observed phase sampling deviates from that of uniform phase sampling. The variance is normalized such that zero variance corresponds to the case where the light curve is uniformly sampled.

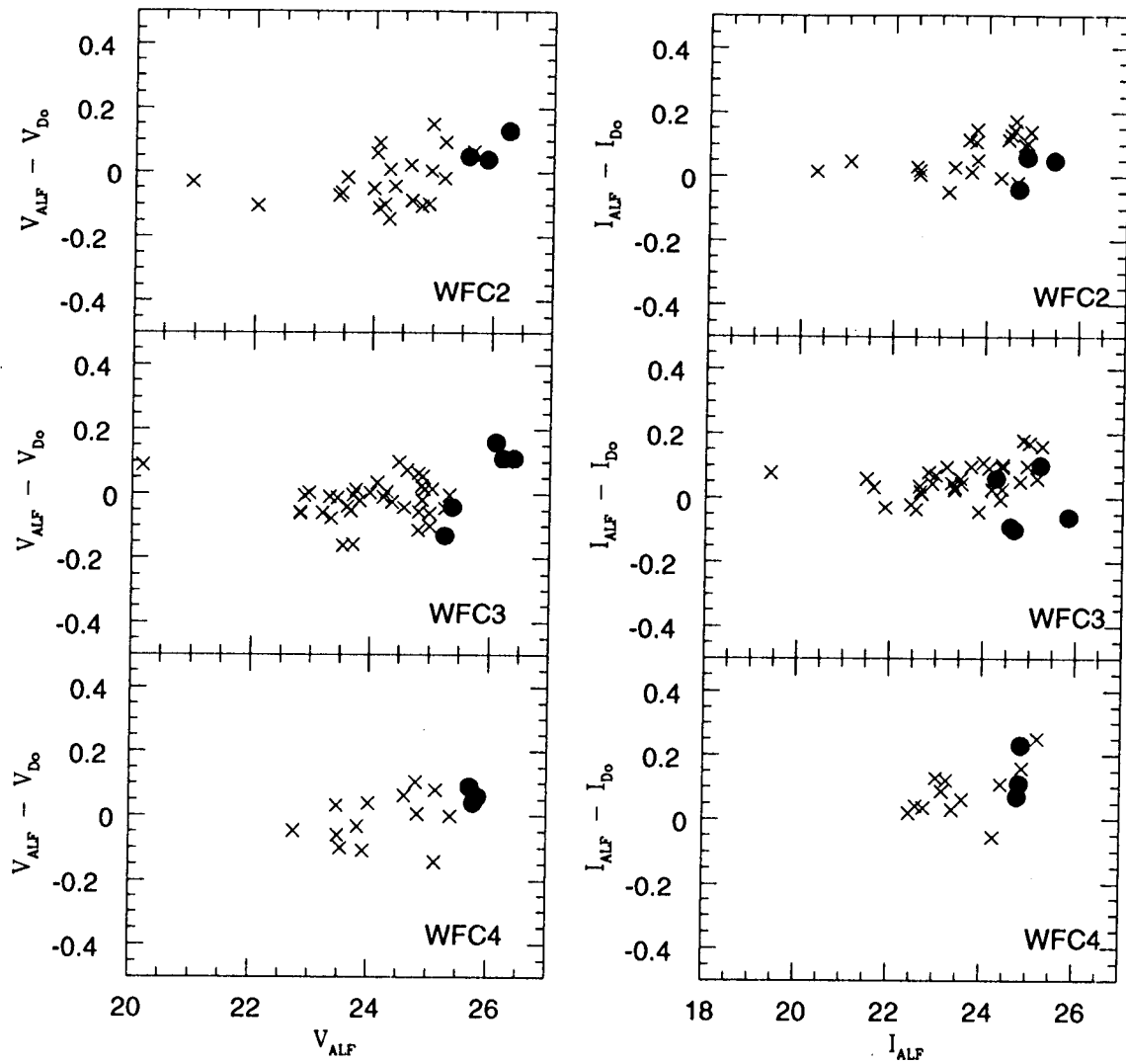


Fig. 4.— Comparison of ALLFRAME and DoPHOT intensity-averaged magnitudes for secondary standard stars and Cepheid candidates located on chips 2 through 4. Standard stars from Table 3 are represented by crosses and Cepheid candidates by solid circles.

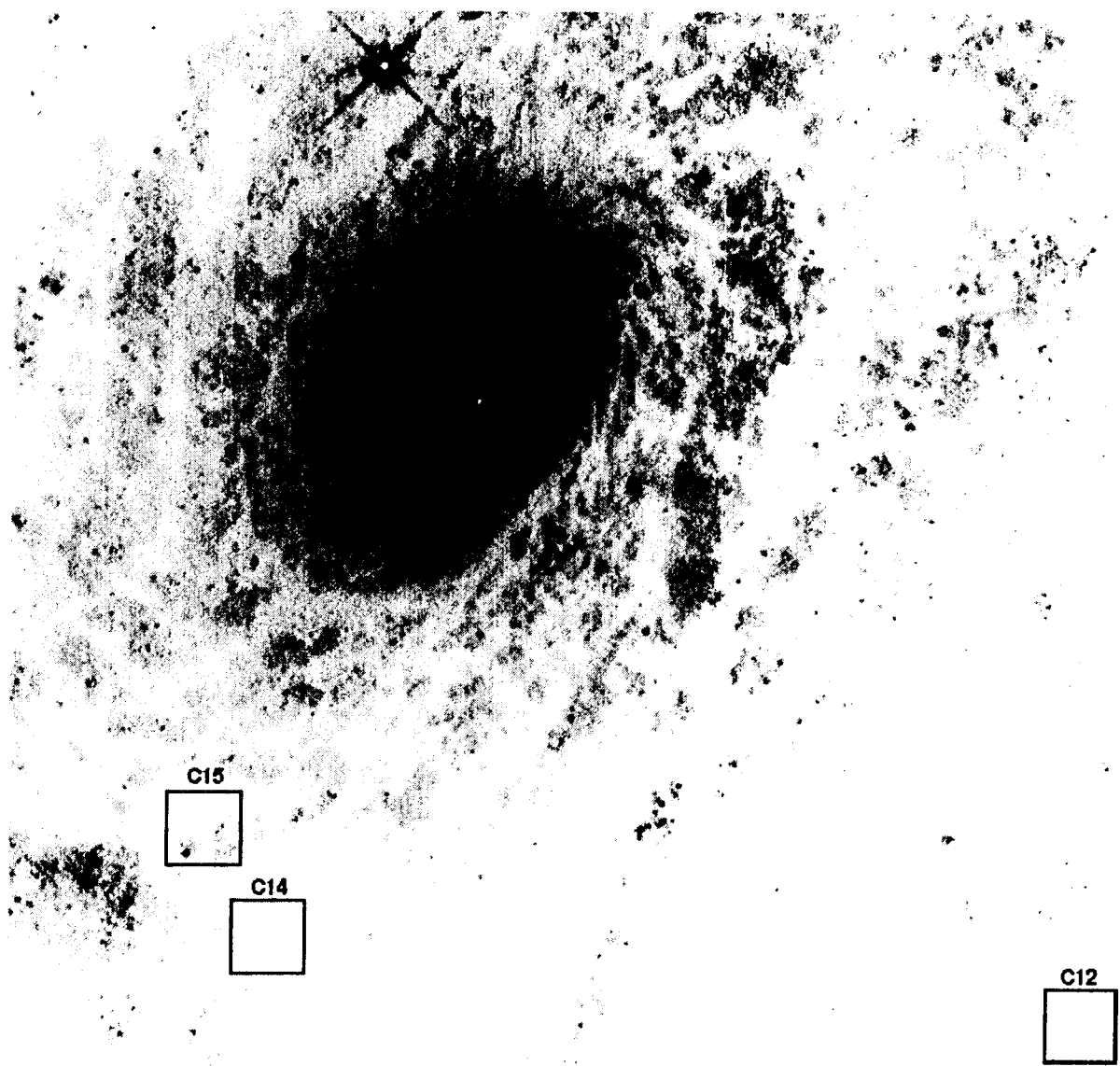


Fig. 5a.— The PC field of view in NGC 4414. Marked are the locations of the variable candidates' fields shown in detail in Figure 12. North is toward the bottom, and east to the right.

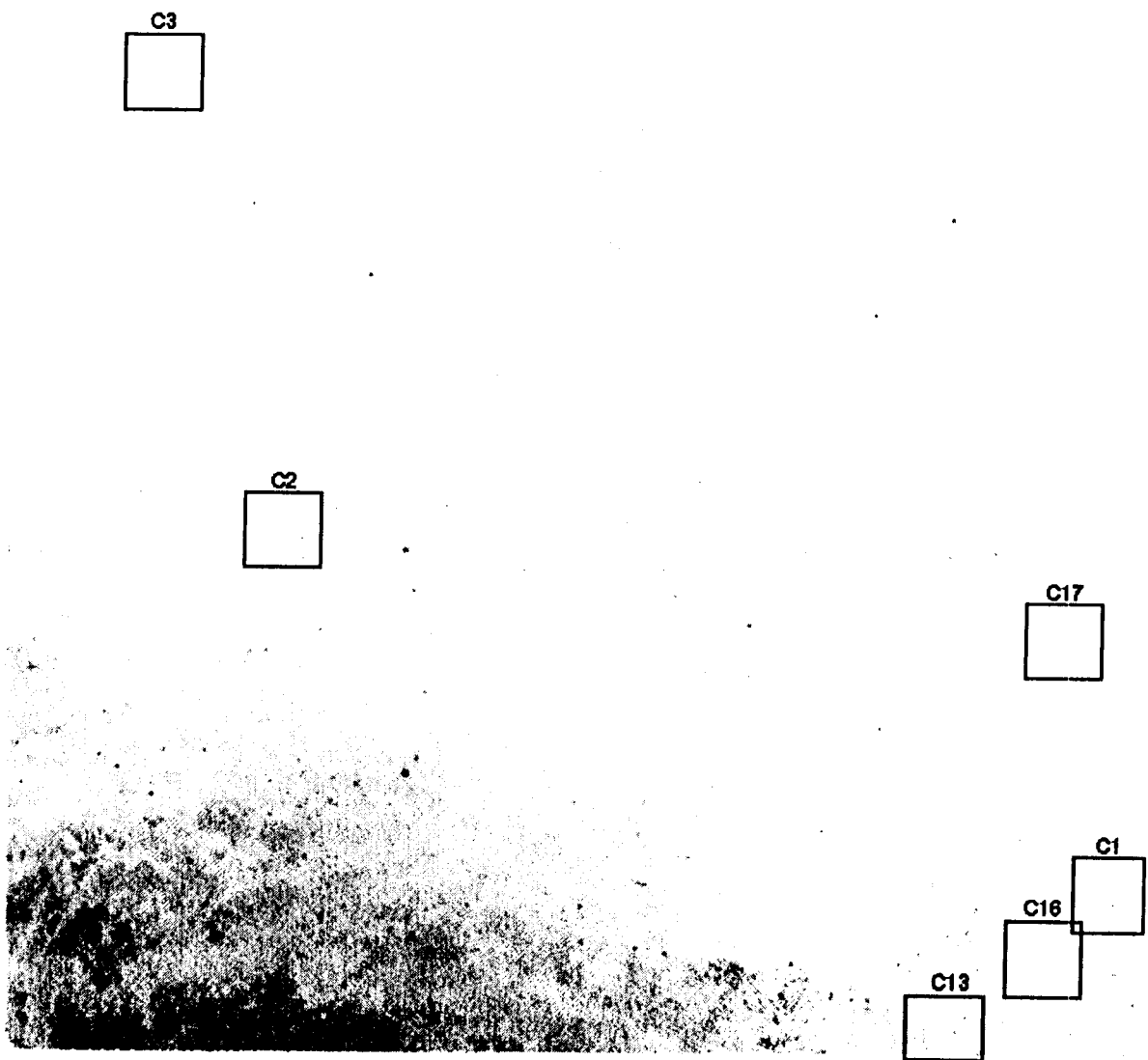


Fig. 5b.— The WFC2 field of view in NGC 4414. Marked are the locations of the variable candidates' fields shown in detail in Figures 6 and 12. North is toward the left, and east to the bottom.

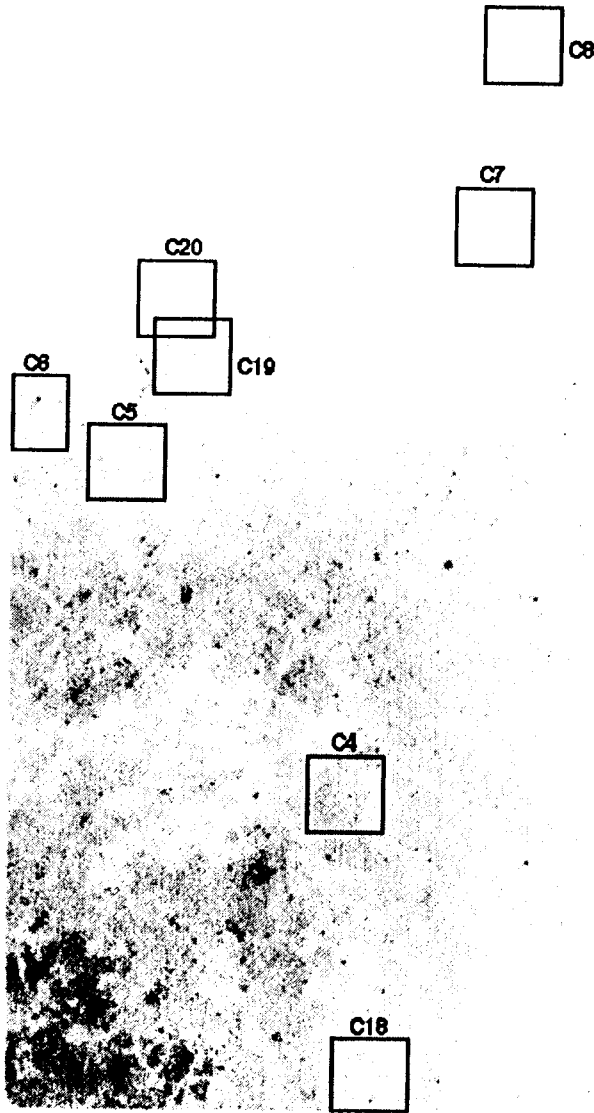


Fig. 5c.— The WFC3 field of view in NGC 4414. Marked are the locations of the variable candidates' fields shown in detail in Figures 6 and 12. North is toward the top, and east to the left.

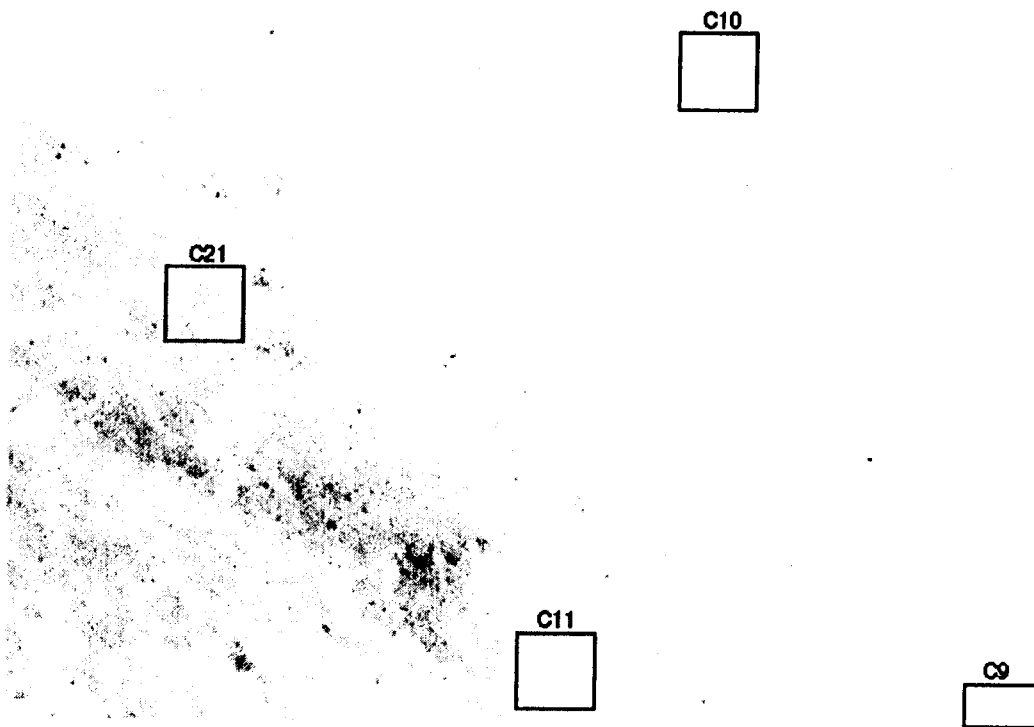


Fig. 5d.— The WFC4 field of view in NGC 4414. Marked are the locations of the variable candidates' fields shown in detail in Figures 6 and 12. North is toward the right, and east to the top.

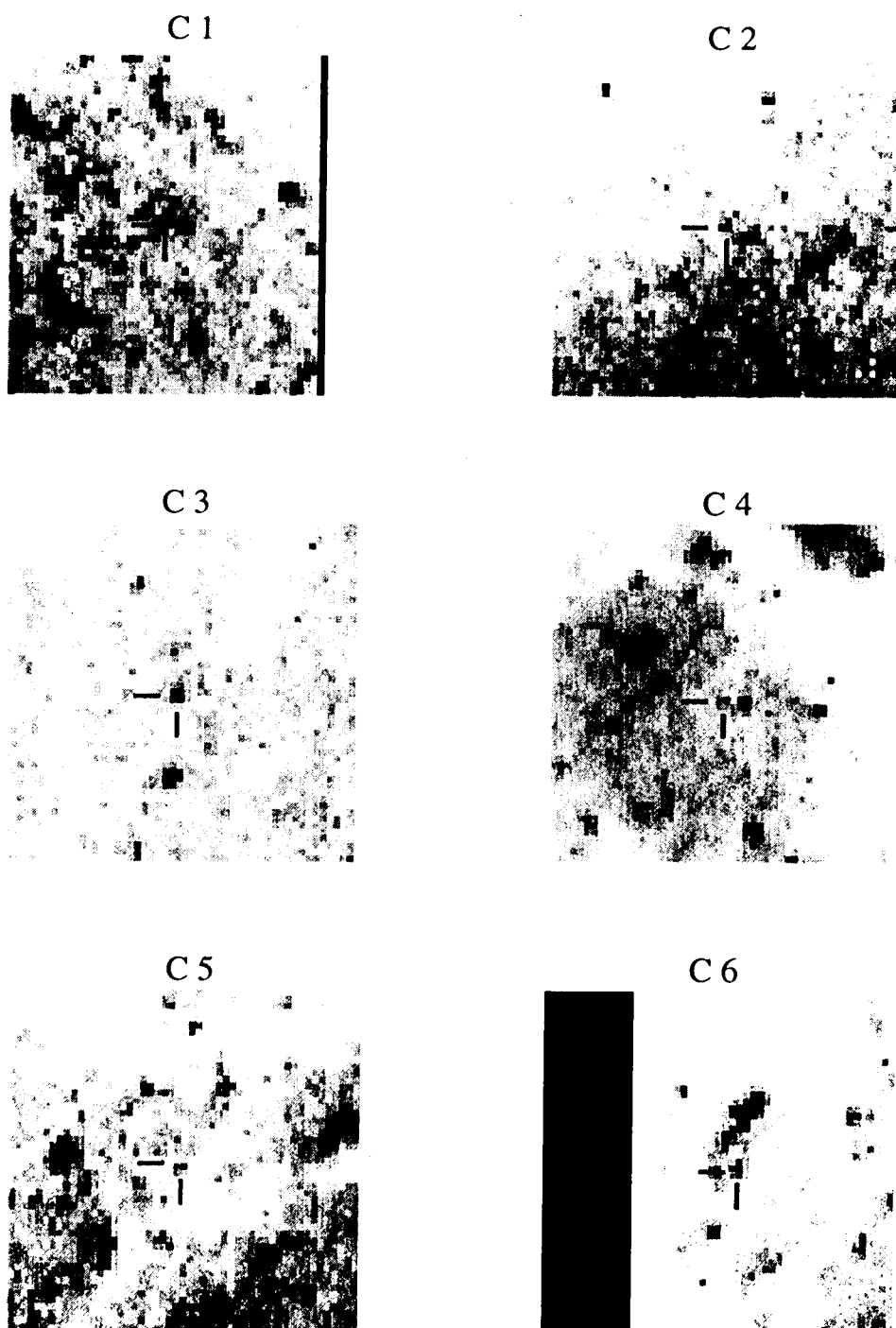


Fig. 6a.— Finder charts for each of the Cepheid candidates. Each image is  $51 \times 51$  pixels, corresponding to  $5''$ . Orientation of each image is as in Figure 5.

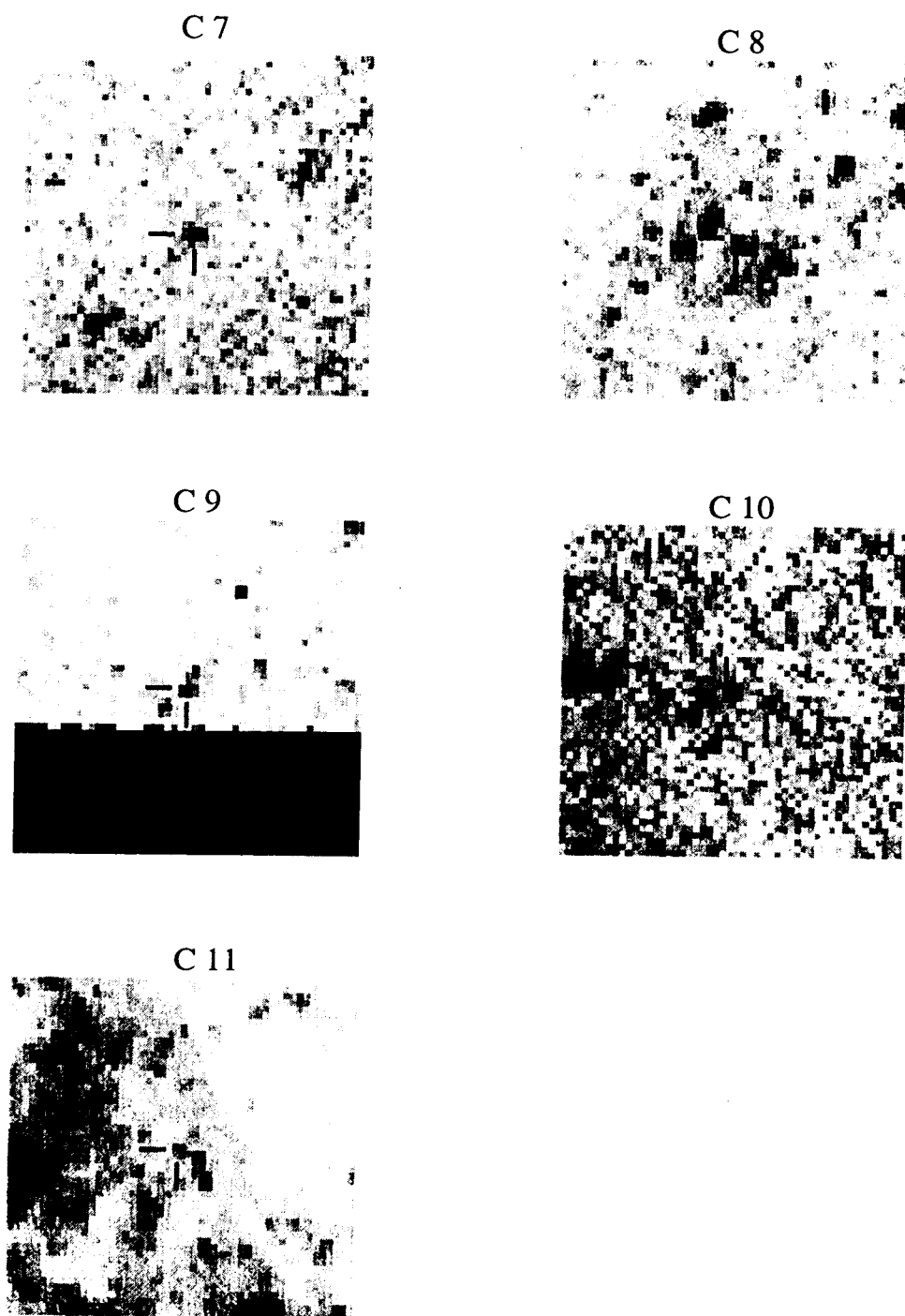


Fig. 6b.— Finder charts for each of the Cepheid candidates. Each image is  $51 \times 51$  pixels, corresponding to  $5''$ . Orientation of each image is as in Figure 5.

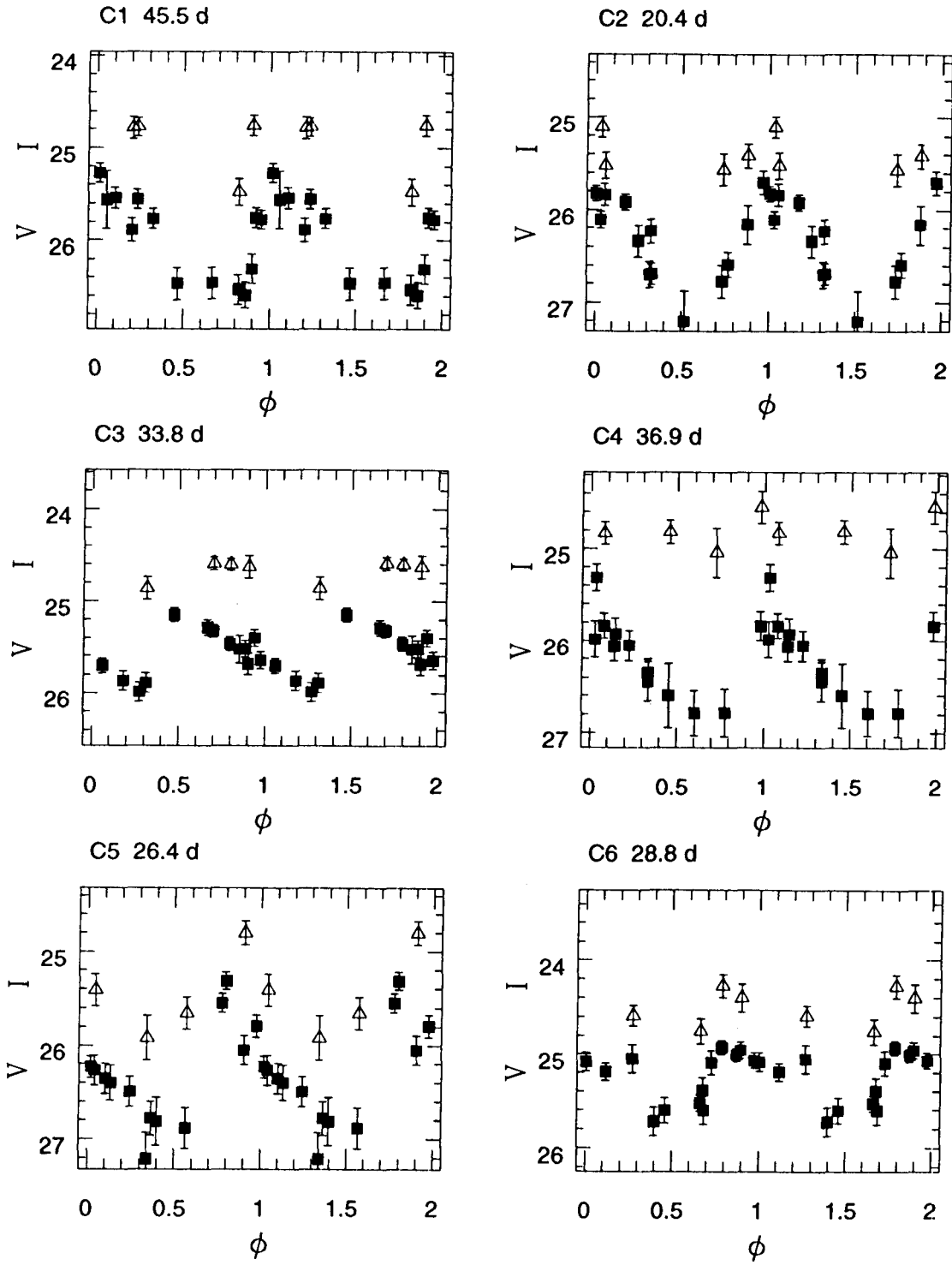


Fig. 7a.— Light curves for each of the 11 Cepheid candidates. The  $V$  magnitudes are plotted as solid circles, and  $I$  as open triangles. Data are plotted over a second cycle for clarity.

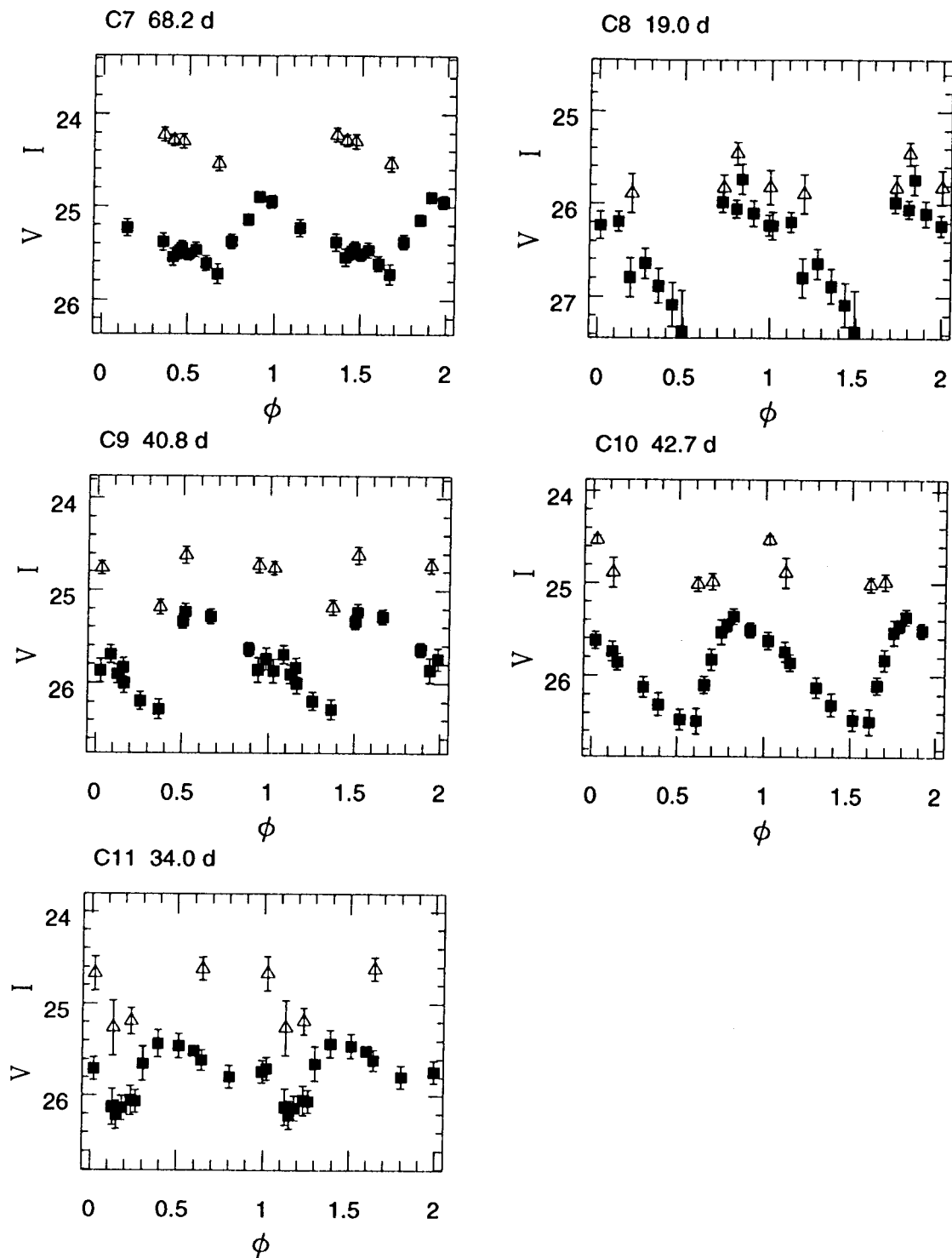


Fig. 7b.— Light curves for each of the 11 Cepheid candidates. The  $V$  magnitudes are plotted as solid circles, and  $I$  as open triangles. Data are plotted over a second cycle for clarity.

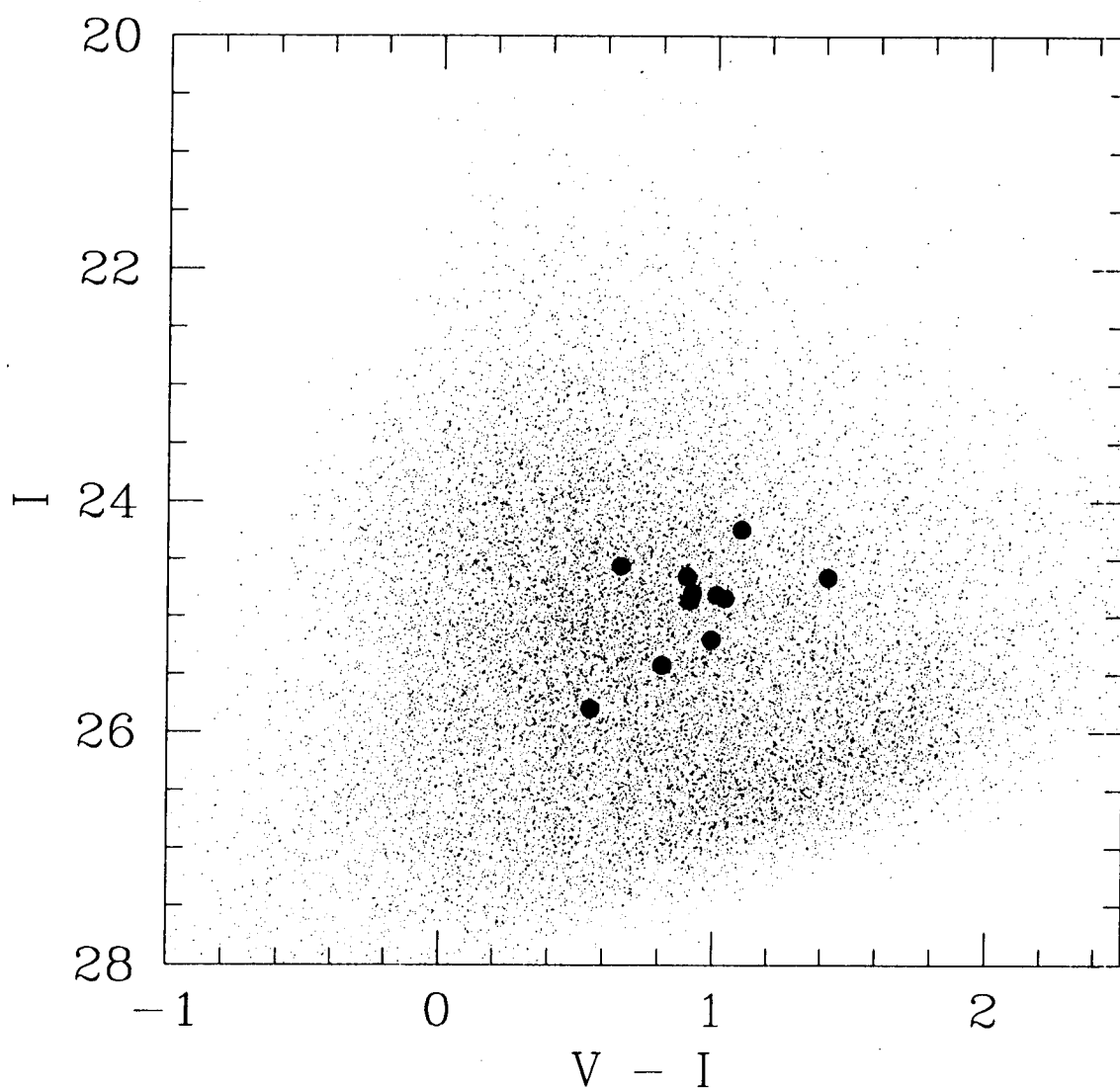


Fig. 8.—  $I$  vs.  $V - I$  color-magnitude diagram for the 3 WFC chips. Phase weighted  $I$  magnitude and color are plotted for each of the Cepheid candidates as solid circles.

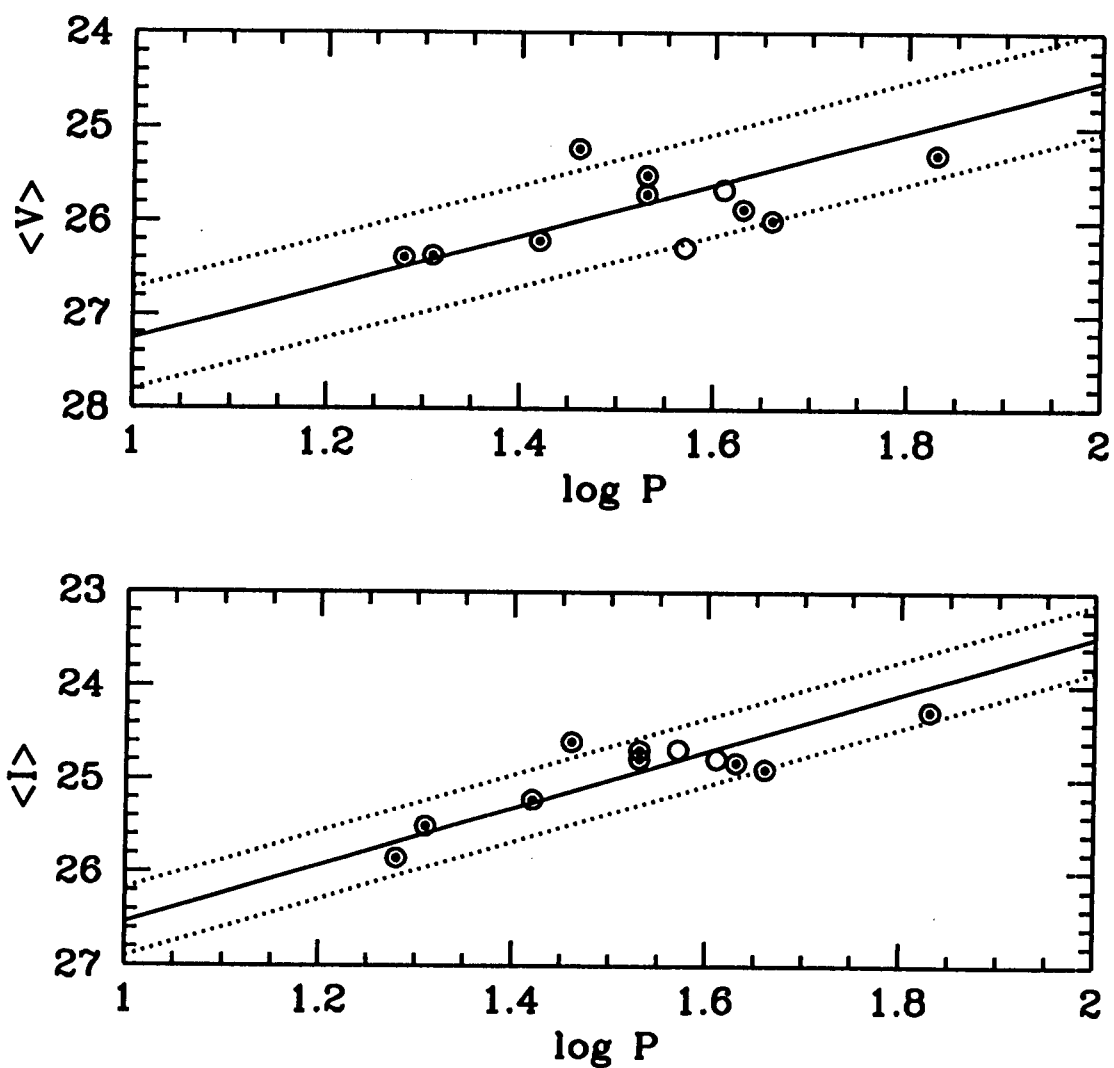


Fig. 9.— The  $V$  and  $I$  PL relations for the Cepheids listed in Table 6. The solid line represents the best fit to the NGC 4414 data. The dotted lines represent the scatter expected due to the intrinsic width of the Cepheid instability strip. Cepheid candidates excluded from the fit are plotted as open circles.

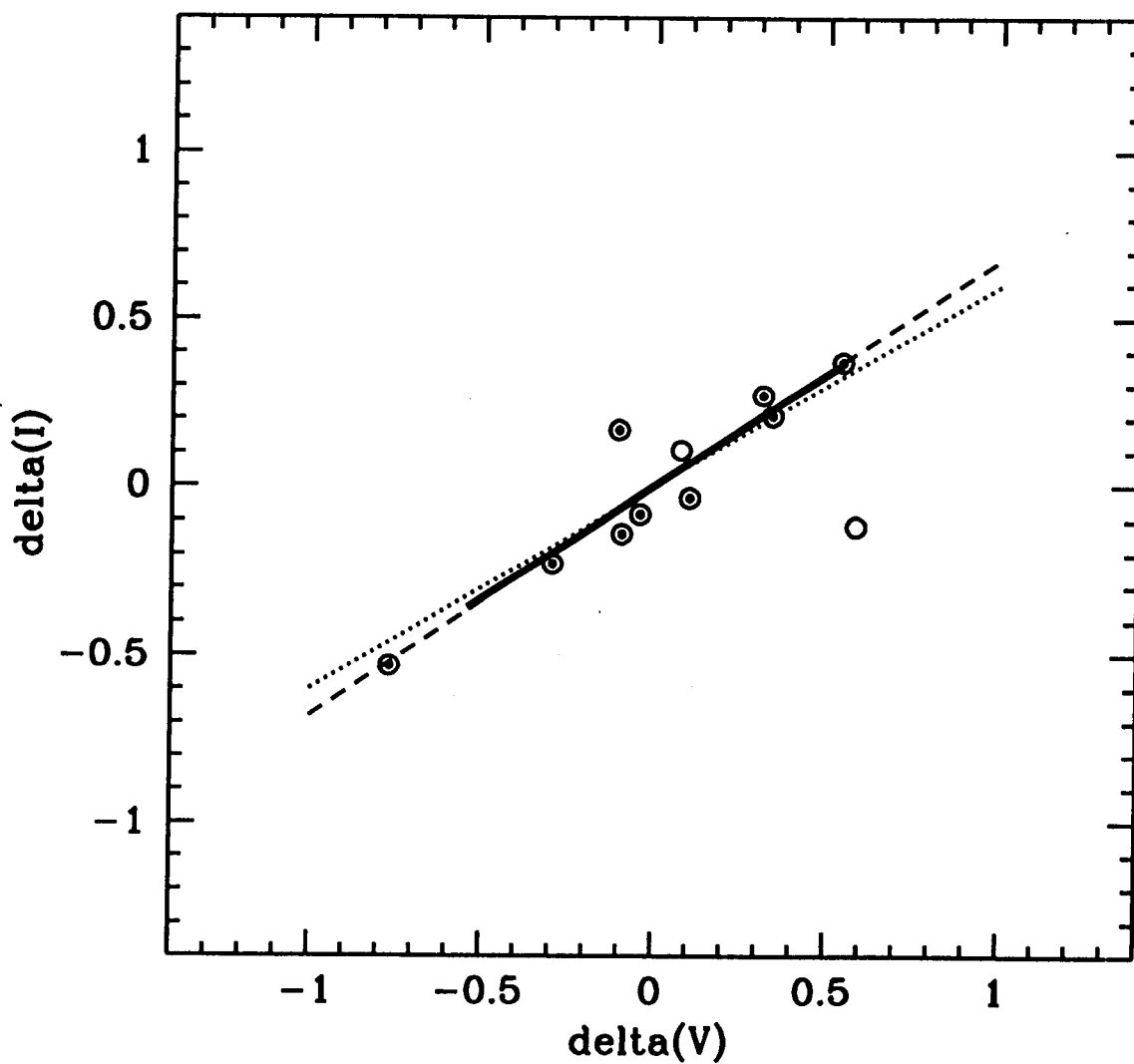


Fig. 10.— Magnitude residuals in  $I$  and  $V$  from the PL relations for Cepheids in NGC 4414. Cepheids excluded from the fit are represented as open circles. The expected scatter due to the intrinsic width of the instability strip is represented by the solid line. The correlation expected due to differential reddening is given by the dotted line. The dashed line is a fit to the data.

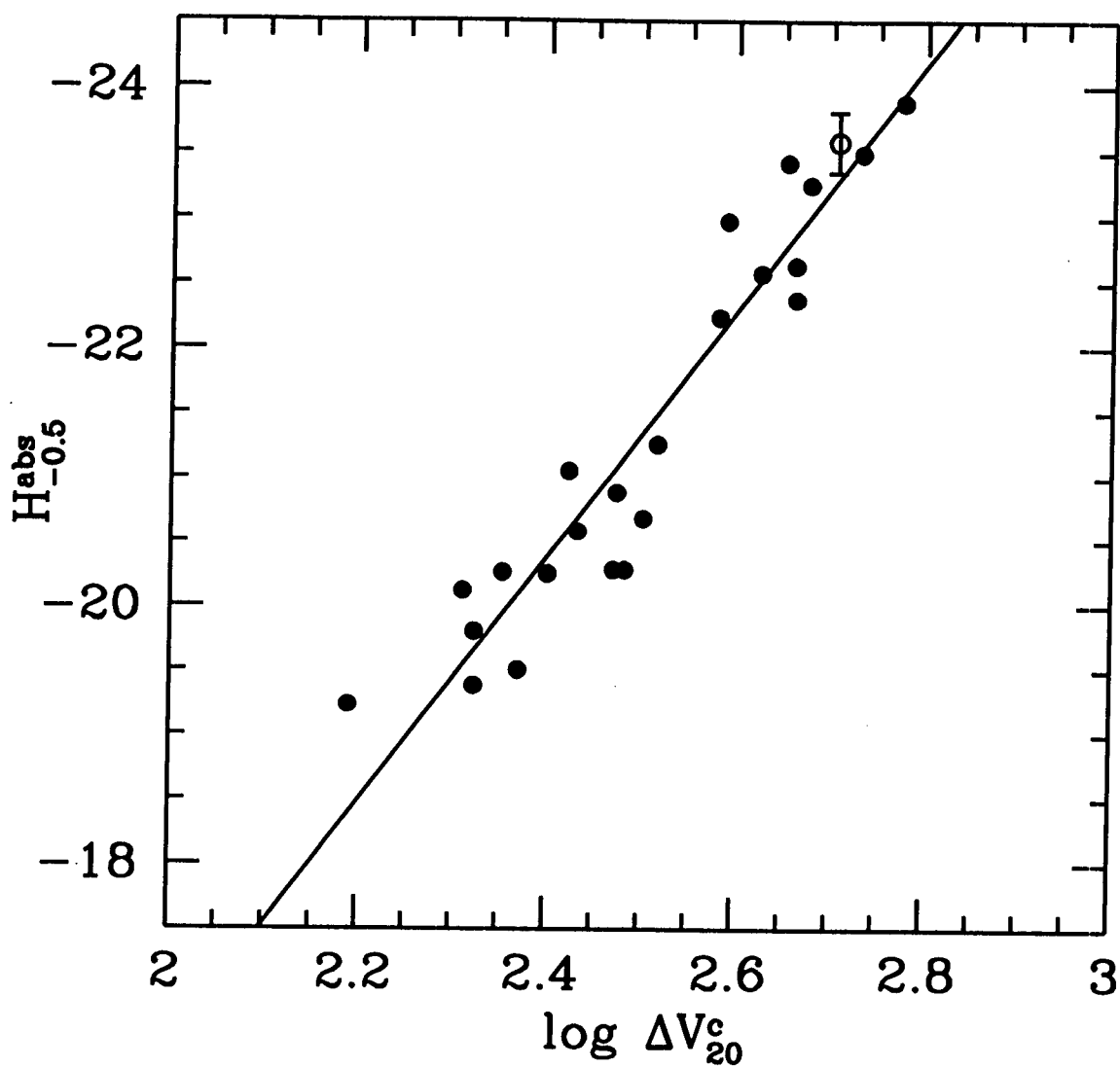


Fig. 11.— The  $H$  band Tully-Fisher relation. Local calibrators from Mould *et al.* (1995) and references therein are plotted as solid circles. NGC 4414 is placed on this plot using the data of Aaronson *et al.* (1982b) and our new distance modulus, and is represented as an open circle with error bars. The line is the  $H$  band TF calibration given by Mould *et al.* (1995).

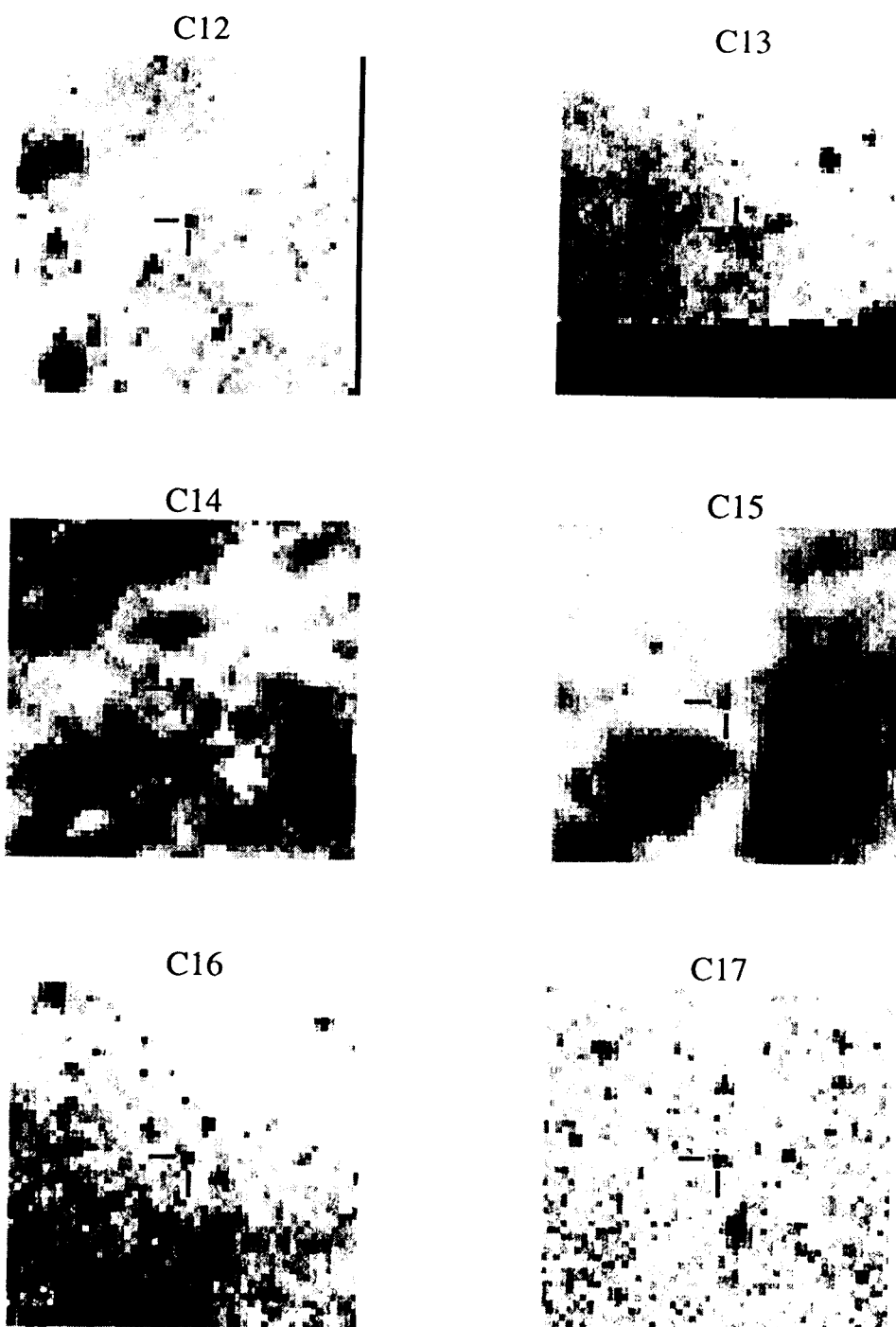


Fig. 12a. — Finder charts for the additional variable candidates. Each image is  $51 \times 51$  pixels, corresponding to  $5''$  for the WFC and  $2''.5$  for the PC (candidates C12, C14, and C15). Orientation of each image is as in Figure 5.